

Final Author Comments to reviewers of amt-2019-195,

- (1) Anonymous Referee #3 (pages 1-3)
- (2) Anonymous Referee #4 (page 5-end)

### **To anonymous Referee #3**

We thank the referee #3 for constructive comments on the manuscript amt-2019-195, “Comparison of Optimal Estimation HDO/H<sub>2</sub>O Retrievals from AIRS with ORACLES measurements.” We have addressed all comments from the referee.

Below are (1) comments from the referee, (2) our author’s response **in bold** and (3) author’s changes in the manuscript.

#### Specific comments

Comment 1:

(1) I48-57: Another instrument that provided HDO measurements was Envisat MIPAS. For instance: Lossow, S., Steinwagner, J., Urban, J., Dupuy, E., Boone, C. D., Kellmann, S., Linden, A., Kiefer, M., Grabowski, U., Glatthor, N., Höpfner, M., Röckmann, T., Murtagh, D. P., Walker, K. A., Bernath, P. F., von Clarmann, T., and Stiller, G. P.: Comparison of HDO measurements from Envisat/MIPAS with observations by Odin/SMR and SCISAT/ACE-FTS, *Atmos. Meas. Tech.*, 4, 1855–1874, <https://doi.org/10.5194/amt-4-1855-2011>, 2011.

**(2) We agree and will add a citation to Envisat/MIPAS and other contemporary satellite instruments that measure stratospheric HDO. This will be placed in the text immediately before the paragraph on satellite retrievals of tropospheric HDO.**

**(3) Changes to text, new paragraph added (I48) and the new references have been added to the end of the manuscript.**

“Early remote sensing of atmospheric HDO was made by the ATMOS (Atmospheric Trace Molecule Spectroscopy) mission on the Space Shuttle (Rinsland et al., 1991; Irion et al., 1996; Moyer et al., 1996; Kuang et al., 2003), retrieving in the upper troposphere/lower stratosphere. Global stratospheric HDO measurements have been provided by satellite instruments including Envisat/MIPAS (Michelson Interferometer for Passive Atmospheric Sounding) (Steinwagner et al., 2007, 2010; Lossow et al., 2011), Odin/SMR (Sub-Millimetre Radiometer) (Murtagh et al., 2002; Urban et al., 2007), and SCISAT-1 (Scientific Satellite)/ACE-FTS (Atmospheric Chemistry Experiment fourier transform spectrometer) (Bernath et al., 2005; Nassar et al., 2007; Lossow et al., 2011; Randel et al., 2012). Atmospheric columns densities of HDO and H<sub>2</sub>O have been retrieved from Sentinel-5 Precursor/TROPOMI (Tropospheric Monitoring Instrument) (Schneider et al., 2020).”

Comment 2:

(1) I130-131: Are these mean winds and surface pressure during the aircraft campaign (September 2016) or do they refer to a specific date and time?

**(2) These are mean winds and surface pressure from MERRA2. We will modify a sentence in the Figure 1 caption.**

**(3) Changes to text, modified Figure 1 caption:**

“Superimposed on the map are the September 2016 monthly mean 700-hPa winds (white vectors) and surface pressure (white isobars), along with the approximate biomass burning region (green rectangle).”

Comment 3:

(1) I243-256: If it is not too much extra work, I would suggest to combine Figs. 2 and 3 in a single figure, e.g., by using different colors for the different matching criteria.

**(2) We will combine Figures 2&3 with loose-constraint AIRS FOV (open squares) and close-constraint AIRS FOV (solid black squares).**

Comment 4:

(1) I291-292: Adjust y axis range to -200 ... +6200 m (or similar)?

**(2) We have changed the y axis range accordingly.**

**(3) Revised Figure 4 (formerly Figure 5).**

Comment 5:

(1) I299-300: The caption says "RMS (standard deviation)", but  $\text{RMS}^2 = \text{BIAS}^2 + \text{STDDEV}^2$ , I think? Are these numbers standard deviations or RMS errors?

**(2) These numbers are standard deviations. The convention in our community has been to not include bias in the RMS. We will clarify in the text that bias is not included in our RMS calculations.**

(3) New sentence added to Table 2 caption: “The reported RMS here is the standard deviation, not including the bias.”

Comment 6:

(1) I315: It may help the reader to say that  $G_R$  refers to the gain matrix of the HDO/H<sub>2</sub>O retrieval.

**(2) We have modified the text accordingly.**

(3) Text modified to, “where  $G_R = (G_z^D - G_z^H)$  is the gain matrix of the HDO/H<sub>2</sub>O retrieval”.

Comment 7:

(1) I316: Which systematic errors and interference errors have been considered here?

**(2) We have considered random error due to noise, and radiative interference errors due to CH<sub>4</sub>, N<sub>2</sub>O, surface emissivity, effects of temperature, and clouds.**

(3) New sentence added: “Interference errors are due to CH<sub>4</sub>, N<sub>2</sub>O, surface emissivity, effects of temperature, and clouds.”

Comment 8:

(1) I316-318: Looking at the averaging kernels, there are likely quite significant correlations being found in retrieval covariance  $S$ ?

**(2) Yes, the reviewer is correct. All of our retrieval products have significant covariation between levels and species but these are taken into account for process studies by appropriate use of the supplied uncertainties and in assimilation studies through use**

**of the averaging kernel and observation error covariances in the assimilation cost function.**

(3) No change to the text.

Comment 9:

(1) l333-334: [Figure caption] Maybe say again that the estimated error is obtained from optimal estimation retrieval theory and the empirical error is obtained from the satellite-aircraft comparison, to help the reader?

(2) **We have modified the text accordingly.**

(3) New sentence added to figure caption: "The empirical error is obtained from the statistics of the satellite-aircraft comparison, while the estimated error is obtained from optimal estimation retrieval theory."

Comment 10:

(1) l344-348: Based on these error estimates, can the AIRS HDO/H<sub>2</sub>O ratio retrievals be considered useful for further scientific analysis?

(2) **Yes, the AIRS HDO/H<sub>2</sub>O ratio retrievals are useful for scientific analysis. We will clearly state this in the Conclusions.**

(3) New sentence added to end of Conclusions, "The errors are sufficiently small that the AIRS HDO/H<sub>2</sub>O ratio retrievals are useful for scientific analysis. This long term global data record has much potential utility."

Comment 11:

(1) l357-359: Not sure the team list is actually needed?

(2) **The AMT publication guide specifies to use this format.**

(3) No change to the text.

Technical corrections - **We have made all technical corrections as listed below:**

l24 and l44: ... HDO/H<sub>2</sub>O \_ratio\_

l81: D/H -> HDO/H<sub>2</sub>O

l85, l138, l226, l270 and other places: use lower case section headings

l151: \_the\_ forward model

l169: DeSouza-Machado

l176: of \_the\_ satellite retrievals

l213: completed \_by\_ applying

l258-259: Labels (a) and (b) are missing: **We have added labels (a) and (b) to Figure 3 (formerly Figure 4).**

l332: shows \_that\_ the empirical error

l340-341: acronym for WISPER does not need to be repeated: **acronym deleted.**

l467: paper title is formatted as a hyperlink: **hyperlink removed.**

We have also discovered the following typographical errors and corrected them:

p. 3, line 55 and p. 5 line 96: change Level 1b to Level **1B**

- p. 4, line 71: Change Fu et al., 2013 to **R.** Fu et al., 2013.
- p. 5, line 96: Change Level 1b (L1b) to 'Level 1B (L1B)'
- p. 8 line 141: Change Fu et al. 2013 to **D.** Fu et al., 2013).

#### **To anonymous Referee #4**

We thank the referee #4 for constructive comments on the manuscript amt-2019-195, "Comparison of Optimal Estimation HDO/H<sub>2</sub>O Retrievals from AIRS with ORACLES measurements." We have addressed all comments from the referee.

Below are (1) comments from the referee, (2) our author's response **in bold** and (3) author's changes in the manuscript.

#### **Specific comments**

Comment 1:

- (1) Lines 92-93: Is AMSU used in the retrieval in any way? Not sure you really need to include its introduction here as you are not using the golf ball configuration (9xAIRs + 1xAMSU IFOV).
- (2) The reviewer is correct that the AIRS HDO retrieval does not use AMSU.**
- (3) Section 2.1 text has been modified to remove the 2-sentence introduction to AMSU. Instead, one sentence defines the horizontal resolution: "These footprint observations have a horizontal resolution of approximately 13.5 km at nadir."

Comment 2:

- (1) Line 116: The reference for WISPER, if still in preparation are there any additional technical reports etc that could also be added?
- (2) The reference for WISPER is still in preparation. AMT allows the gray literature (e.g. conference proceedings) if nothing else is available so we additionally cite an AGU abstract, Henze et al. 2017.**
- (3) New citation added: Henze and Noone, 2017, Henze, D., and Noone, D.: *The Dependence of Entrainment and Drizzle in Marine Stratiform Clouds on Biomass Burning Aerosols Derived from Stable Isotope and Thermodynamic Profiles*, AGU Fall Meeting, New Orleans, Louisiana, United States, Abstract A11C-0048, 2017.

Comment 3:

- (1) Table 1: Why are there some large discrepancies between the number of collocations and others have lower or no reduction in matchups when the tighter lat/lon constraint is applied? Maybe some additional information for context in the table header would be useful for readers unfamiliar with the ORACLES campaign.
- (2) The reviewer has a good point. It should be better explained here that the loose constraint is a large rectangle aligned with parallels of latitude and meridians of longitude. All flights except two (Sep 2, 2016, and Sep 14, 2016) had large rectangles because the aircraft flew along the diagonal of the rectangle (see Figure 2). Sep. 2 and Sep. 14, 2016, had different flight patterns so we used smaller latitude/longitude shapes to constraint AIRS data on those days. The tighter constraint is matched AIRS geolocations and aircraft FOVs within 0.3 degrees of each other.**
- (3) New text has been added to the body of Sec. 4.1:

We have replaced the text “Within each flight are several profiles each spanning 1 to 3 degrees (or ~ 100 to 300 km), so measurement pairs are typically within 3 degrees (Fig. 2).”

With the revised text:

“The loose constraint (Table 1 column 1, Fig. 2 open circles and Fig. 4a) is that, for an aircraft vertical profile (~ 100 to 300 km in length), all AIRS geolocations within the same rectangle of maximum to minimum latitude and maximum to minimum longitude are selected. The only exceptions were the aircraft flights of 9/2/2016 and 9/14/2016, which had different flight patterns and smaller shapes were used to constrain AIRS geolocations. The tighter constraint (Table 1 column 2, Fig. 2 closed circles and Fig. 4b) is to match only AIRS geolocations within 0.3 degrees (30 km) of the aircraft flight track.”

Comment 4:

- (1) Line 222-223: Do you get 1 DOF between 750-350 hPa?
- (2) Yes, most retrievals have approximately 1 DOF between 750-350 hPa. Most of the sensitivity of AIRS to HDO is at pressure levels of 750 hPa to 350 hPa so most of the information is coming from these levels.
- (3) No change to text.

Comment 5:

- (1) Line 239: Is the DOF threshold for a sub-column between 750-350 hPa?
- (2) No, the DOF threshold is for the total column of AIRS HDO/H<sub>2</sub>O. This DOF threshold is used merely as a way to filter for the retrievals with the highest information content.
- (3) New Text added to Section 4.1:  
“Following Worden et al. (2007) and Brown et al. (2008), we filter data for a reasonable threshold of standard nadir data product DegreesOfFreedomForSignal (DOFS) > 1.1, but include all values of AverageCloudEffOpticalDepth. Data product DOFS is the trace of the averaging kernel, and is a measure of the number of independent parameters for the retrieved HDO/H<sub>2</sub>O profile. AverageCloudEffOpticalDepth is the retrieved cloud mean optical depth at wavenumbers from 975 to 1200 cm<sup>-1</sup> from the final retrieval step (e.g., the same for all species) (Kulawik et al., 2006).”

Comment 6:

- (1) Line 240: Where does the cloud optical depth information come from? Is it a retrieval output? Is there any uncertainty information associated with the cloud information, if so is it propagated?
- (2) The cloud optical depth is standard retrieval output, retrieved for a non-scattering cloud reported from the values at the final sequential retrieval step. The uncertainty information associated with the cloud is propagated. The AIRS cloud optical depth is retrieved the same way as the TES cloud optical depth, new citation: Kulawik, S. S., Worden, J., Eldering, A., Bowman, K., Gunson, M., Osterman, G. B., Zhang, L., Clough, S., Shephard, M. W. and Beer, R.: Implementation of cloud retrievals for Tropospheric Emission Spectrometer (TES) atmospheric retrievals: part 1. Description and characterization of errors on trace gas retrievals, *J. Geophys. Res.*, 111, D24204, doi:10.1029/2005JD006733, 2006.

- (3) New text, New sentence added: "Interference errors are due to CH<sub>4</sub>, N<sub>2</sub>O, surface emissivity, effects of temperature, and clouds."  
And also new text in Section 4.1,  
"Following Worden et al. (2007) and Brown et al. (2008), we filter data for a reasonable threshold of standard nadir data product DegreesOfFreedomForSignal (DOFS) > 1.1, but include all values of AverageCloudEffOpticalDepth. Data product DOFS is the trace of the averaging kernel, and is a measure of the number of independent parameters for the retrieved HDO/H<sub>2</sub>O profile. AverageCloudEffOpticalDepth is the retrieved cloud mean optical depth at wavenumbers from 975 to 1200 cm<sup>-1</sup> from the final retrieval step (e.g., the same for all species) (Kulawik et al., 2006)."

Comment 7:

- (1) Figures 23: A little colour/shading would be useful to help distinguish land/ocean. It is difficult to see the aircraft track through the AIRS IFOV markers. How many aircraft profiles are each subfigure?  
(2) We will modify the Figures 2 and 3 to be easier to read. There are typically 3 to 6 aircraft profiles per subfigure. They overlap spatially as the aircraft flies the same diagonal path.

Comment 8:

- (1) Figure 4: Subfigure headings are missing (a,b).  
(2) We have added the subfigure headings (a) and (b) to the figure.  
(3) Revised Figure, now renumbered as Figure 3.

Comment 9:

- (1) Line 288: Little or no difference to a priori between 800 hPa-surface, is AIRS really adding anything here in the PBL? Is the averaging kernel not setting the difference between  $(x - x_a)$  residual to/or close to zero?  
(2) The reviewer has an excellent point. In most cases AIRS does not have much sensitivity to the PBL deuterium content. Any differences between the PBL *a priori* will therefore reflect the diagonal of the averaging kernel, plus the cross terms that describe the sensitivity of the PBL estimate to the true state in the rest of the atmosphere.  
(3) Since in most cases AIRS does not have much sensitivity to PBL HDO, we have modified the line 343-344 in the manuscript,  
"We have shown that AIRS-only retrievals have sensitivity to HDO from the middle troposphere to the boundary layer."  
to:  
"We have shown that AIRS-only retrievals have sensitivity to HDO in the middle and lower troposphere."

Comment 10:

- (1) Section 5: Is this a description of the a posteriori error? When you say you are characterising the error budget I would expect some account of the collocation/

representativeness uncertainty due to the mismatch with the aircraft. I think you might just need to change the wording on line 305 to make this clearer.

**(2) Our response to the reviewer is, yes, we are referring to the *a posteriori* error. We will make the wording on lines 305 and 325-327 clearer as detailed below.**

(3) At the start of Section 5. Error Estimation, we will modify:

"... we characterize the error budget for AIRS and assess this error by comparison with the ORACLES aircraft measurements."

To:

"... we characterize the *a posteriori* error budget for AIRS HDO/H<sub>2</sub>O and assess this error by comparison with the ORACLES aircraft measurements."

At lines 325-327, discussing differences between the estimated error from OE and empirical error from the comparison, we will modify

"These differences are likely due to atmospheric variability as we do not have exact matchups between the AIRS data and aircraft measurements."

To:

"These differences between the OE estimated error and the empirical error are likely due to uncertainties in atmospheric variability in space and time and in the collocation between satellite retrieval and aircraft measurements. The instrument operator (Eq. 1) accounts for error due to the mismatch in \*vertical\* sensitivity between the satellite retrieval and aircraft *in situ* vertical profiling. In the cases where AIRS is compared to *in situ* measurements without the instrument operator, there is an additional smoothing error (Table 2). The instrument operator does not account for error due to \*horizontal\* mismatch. The close coincidences are all within 30 km (0.3 degrees), but given time differences, and the AIRS 15-km nadir footprint and limited *in situ* measurement, the satellite and aircraft are not necessarily measuring the same air mass. There is a collocation error on the order of ~10 per mil due to horizontal collocation/representativeness uncertainty."

#### Technical Comments

(1) Line 206: *in situ* – should be in italics

**(2) We have made *in situ* italicized every time it appears in the manuscript.**



1 **Title Page**

2

3 **Comparison of Optimal Estimation HDO/H<sub>2</sub>O Retrievals**  
4 **from AIRS with ORACLES measurements**

5 **Robert L. Herman<sup>1</sup>, John Worden<sup>1</sup>, David Noone<sup>2,3</sup>, Dean Henze<sup>2</sup>, Kevin**  
6 **Bowman<sup>1</sup>, Karen Cady-Pereira<sup>4</sup>, Vivienne H. Payne<sup>1</sup>, Susan S. Kulawik<sup>5</sup>, and**  
7 **Dejian Fu<sup>1</sup>**

Deleted: 3  
Deleted: 4

8 [1] Jet Propulsion Laboratory, California Institute of Technology, Pasadena, California,  
9 USA.

10 [2] College of Earth, Ocean, and Atmospheric Sciences, Oregon State University,  
11 Corvallis, Oregon, USA.

12 [3] [Now at Department of Physics, University of Auckland, Auckland, New Zealand.](#)

13 [4] Atmospheric and Environmental Research, Inc. (AER), Lexington, Massachusetts,  
14 USA.

15 [5] Bay Area Environmental Research Institute, Petaluma, California, USA.

Deleted: 4

16 Correspondence to: R. L. Herman ([Robert.L.Herman@jpl.nasa.gov](mailto:Robert.L.Herman@jpl.nasa.gov))

17 © 2020. All rights reserved.

21 **Abstract**

22 In this paper we evaluate new retrievals of the deuterium content of water vapor from the  
23 Aqua Atmospheric InfraRed Sounder (AIRS) with aircraft measurements of HDO and  
24 H<sub>2</sub>O from the ObseRvations of Aerosols above Clouds and their intEractionS  
25 (ORACLES) field mission. Single footprint AIRS radiances are processed with an  
26 optimal estimation algorithm that provides vertical profiles of the HDO/H<sub>2</sub>O ratio,  
27 characterized uncertainties, and instrument operators (i.e., averaging kernel matrix).  
28 These retrievals are compared to vertical profiles of the HDO/H<sub>2</sub>O ratio from the Oregon  
29 State University Water Isotope Spectrometer for Precipitation and Entrainment Research  
30 (WISPER) on the ORACLES NASA P-3B Orion aircraft. Measurements were taken over  
31 the Southeast Atlantic Ocean from 31 August to 25 September 2016. HDO/H<sub>2</sub>O is  
32 commonly reported in  $\delta D$  notation, which is the fractional deviation of the HDO/H<sub>2</sub>O  
33 ratio from the standard reference ratio. For collocated measurements, the satellite  
34 instrument operator (averaging kernels and a priori constraint) is applied to the aircraft  
35 profile measurements. We find that AIRS  $\delta D$  bias relative to the aircraft is well within  
36 the estimated measurement uncertainty. In the lower troposphere, 1000 to 800 hPa, AIRS  
37  $\delta D$  bias is -6.6‰ and the Root Mean Square (RMS) deviation is 20.9‰, consistent with  
38 the calculated uncertainty of 19.1‰. In the mid-troposphere, 800 to 500 hPa, AIRS  $\delta D$   
39 bias is -6.8‰ and RMS 44.9‰, comparable to the calculated uncertainty of 25.8‰.

Deleted: a

Deleted: or

42 **1. Introduction**

43 The deuterium content of tropospheric water vapor is sensitive to the different types of  
44 atmospheric moisture sources such as evaporation from the ocean or land and the  
45 processing that occurs during transport such as mixing or condensation (e.g., Craig, 1961;  
46 Dansgaard, 1964; Galewsky et al., 2016). Condensation and precipitation preferentially  
47 remove the heavier HDO isotopologue from the gas phase relative to the parent  
48 isotopologue H<sub>2</sub>O, whereas evaporation of precipitation at lower altitudes in the  
49 atmosphere can enrich HDO relative to H<sub>2</sub>O vapor. These unique, isotopic properties  
50 allow the HDO/H<sub>2</sub>O ratio to be a tracer for the origin, condensation and evaporation  
51 history of an air parcel, thus useful for evaluating changes to the water cycle (e.g.,  
52 Worden et al., 2007; Noone, 2012; Galewsky et al., 2016).

53

54 Early remote sensing of atmospheric HDO was made by the ATMOS (Atmospheric  
55 Trace Molecule Spectroscopy) mission on the Space Shuttle (Rinsland et al., 1991; Irion  
56 et al., 1996; Moyer et al., 1996; Kuang et al., 2003), retrieving in the upper  
57 troposphere/lower stratosphere. Global stratospheric HDO measurements have been  
58 provided by satellite instruments including Envisat/MIPAS (Michelson Interferometer for  
59 Passive Atmospheric Sounding) (Steinwagner et al., 2007, 2010; Lossow et al., 2011),  
60 Odin/SMR (Sub-Millimetre Radiometer) (Murtagh et al., 2002; Urban et al., 2007), and  
61 SCISAT-1 (Scientific Satellite)/ACE-FTS (Atmospheric Chemistry Experiment fourier  
62 transform spectrometer) (Bernath et al., 2005; Nassar et al., 2007; Lossow et al., 2011;  
63 Randel et al., 2012). Atmospheric columns densities of HDO and H<sub>2</sub>O have been  
64 retrieved from Sentinel-5 Precursor/TROPOMI (Tropospheric Monitoring Instrument)

Formatted: Subscript

65 [\(Schneider et al., 2020\)](#).

66

67 In the last decade, satellite retrievals of tropospheric water vapor isotopic composition  
68 (HDO and H<sub>2</sub>O) have been developed, including Envisat/SCIAMACHY (Scanning  
69 Imaging Absorption Spectrometer for Atmospheric Chartography) (Frankenberg et al.,  
70 2009), IASI (Infrared Atmospheric Sounding Interferometer) aboard the MetOp satellites  
71 (Herbin et al., 2009; Schneider and Hase, 2011; Lacour et al., 2012), and TES (the  
72 Tropospheric Emission Spectrometer) on the Aura spacecraft (Worden et al., 2006;  
73 Worden et al., 2007). More recently, Worden et al. have developed HDO retrievals from  
74 the Aqua Atmospheric InfraRed Sounder (AIRS) single footprint Level 1B radiance data  
75 (Worden et al., 2019). These AIRS retrievals are the subject of the present comparison  
76 with aircraft data.

77

78 Satellite HDO measurements have been utilized to study tropical carbon/water feedbacks  
79 (Wright et al., 2017), moist processes in deep convection (e.g. Worden et al., 2007), and  
80 the global partitioning of transpiration to evapotranspiration (Good et al., 2015). A  
81 decadal record of HDO has promise in characterizing global shifts in moisture sources  
82 and atmospheric water balance in response to warming, climactic variability, and land-  
83 use. For example, Bailey et al. (2017) shows that a record of free-tropospheric HDO/H<sub>2</sub>O  
84 would provide an observational constraint on changes in the tropical water balance  
85 (evaporation minus precipitation) in response to shifts in ocean temperature. Wright et al.  
86 (2017) also shows that free-tropospheric deuterium measurements provide a fundamental  
87 new constraint in carbon / water dynamics in the Amazon. They use the TES isotope

Deleted: the isotopic composition of

Deleted: b

90 measurements to show that dry-season evapotranspiration is critical towards initiating the  
91 southern Amazon rainfall, which in turn is critical towards sustaining the Amazon  
92 rainforest (R. Fu et al., 2013). For these reasons a record of the deuterium content of  
93 water vapor from the long (17 years and continuing) record from AIRS holds significant  
94 potential to evaluate changes in the global water cycle.

95  
96 This paper presents detailed comparisons between new AIRS measurements of the  
97 deuterium content of water vapor (or HDO/H<sub>2</sub>O ratio) and accurate *in situ* HDO/H<sub>2</sub>O  
98 measurements from an aircraft sensor during the NASA Observations of Aerosols above  
99 Clouds and their interactions (ORACLES) field mission. In this paper, we denote the  
100 volume mixing ratios  $q_D$  for HDO, and  $q_H$  for H<sub>2</sub>O. By standard convention, we report  
101 the isotopic abundance as  $\delta D$  (per mil or ‰) =  $[(q_D/q_H)_{obs}/(q_D/q_H)_{std} - 1] * 1000$ ,  
102 where  $(q_D/q_H)_{std} = 3.11 \times 10^{-4}$  based on the HDO/H<sub>2</sub>O standard ratio for Vienna Standard  
103 Mean Ocean Water (SMOW).

104

## 105 2. Instrumentation

### 106 2.1 AIRS instrument description

107 The Atmospheric InfraRed Sounder (AIRS) on the NASA Aqua satellite is a nadir-  
108 viewing, scanning thermal infrared grating spectrometer that covers the 3.7 to 15.4  $\mu\text{m}$   
109 spectral range with 2378 spectral channels (Pagano et al., 2003, and Aumann et al.,  
110 2003). Launched on May 4, 2002, Aqua is in a sun-synchronous orbit at 705 km with an  
111 approximately 1:30 pm equator crossing-time as part of the A-Train satellite  
112 constellation. AIRS continues to make daily measurements of most of the globe with its

Deleted: in situ  
Formatted: Font: Not Italic

Formatted: Subscript

Deleted: I  
Deleted: D

116 wide cross-scanning swath of coverage. For HDO retrievals, the single footprint AIRS  
117 Level 1B (LIB) radiances are utilized. These footprint observations have a horizontal  
118 resolution of approximately 13.5 km at nadir. Absolute radiometric accuracy between  
119 220 K and 320 K at all observation angles is better than 0.2 K (Pagano et al., 2003,  
120 2008). The algorithm applied to AIRS radiances to yield HDO is described below in Sect.  
121 3.1.

122

## 123 2.2 WISPER system for aircraft measurements

124 Aircraft measurements were made on the NASA P-3B Orion aircraft during the NASA  
125 ORACLES field mission. ORACLES is a five-year Earth Venture Suborbital (EVS-2)  
126 investigation with three Intensive Observation Periods (IOP) designed to study key  
127 processes that determine the climate impacts of African biomass burning aerosols in  
128 2016, 2017, and 2018. The ORACLES experiment provided multi-year airborne  
129 observations from the NASA P-3B Orion and ER-2 aircraft over the complete vertical  
130 column of the key parameters that drive aerosol-cloud interactions in the southeast  
131 Atlantic Ocean region. The focus of the ORACLES field measurements was a biomass  
132 burning plume that advected west from the African continent to the Atlantic Ocean at 2 to  
133 5 km altitude above sea level, ASL. Here we use data from the ORACLES 2016 IOP  
134 (ORACLES Science Team, 2017), and report on aircraft versus satellite comparisons  
135 from eight flights (Fig. 1 and Table 1).

136

137 Water vapor isotopic abundances ( $\text{HDO}/\text{H}_2\text{O}$  and  $\text{H}_2^{18}\text{O}/\text{H}_2^{16}\text{O}$ ) were measured *in situ* on  
138 the aircraft with the Oregon State Water WISPER system (Water Isotope Spectrometer

**Deleted:** The AIRS instrument makes collocated measurements with the Advanced Microwave Sounding Unit (AMSU) on the Aqua satellite. There are nine AIRS single footprint observations (nadir horizontal resolution of ~13.5 km) arranged in a 3 by 3 grid within a single AMSU footprint of ~45 km (Aumann et al., 2003).

**Deleted:** b

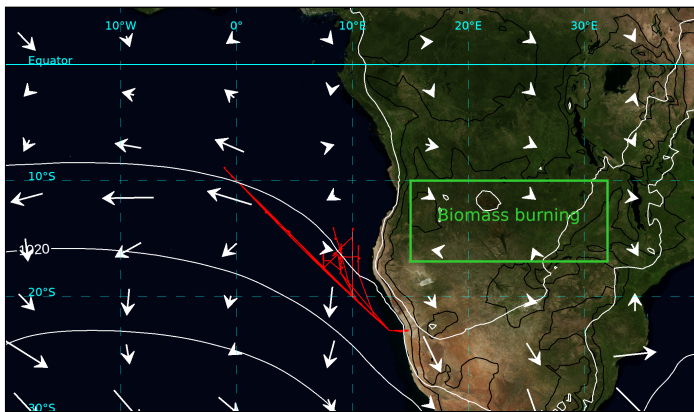
**Deleted:** L1b

**Deleted:** lower troposphere (

**Deleted:** ) above the Atlantic Ocean

**Deleted:** in situ

150 for Precipitation and Entrainment Research, Henze et al., in prep.: [Henze and Noone,](#)  
151 [2017](#)), which uses a modified commercial Picarro L2120-i  $\delta\text{D}/\delta^{18}\text{O}$  Ultra High-Precision  
152 Isotopic Water Analyzer. The measurement technique is cavity ring-down (CRD)  
153 spectroscopy (O’Keefe and Deacon, 1988; Berden et al., 2000; Gupta et al., 2009). The  
154 majority of measurements analyzed in this paper are located within the biomass burning  
155 plume, characterized by elevated  $\text{H}_2\text{O}$  (approximately 6000 ppmv) and elevated  $\delta\text{D}$  (-100  
156 to -70‰). At these abundances of  $\text{HDO}/\text{H}_2\text{O}$ , the 1-Hz precision ( $1\sigma$ ) of the  
157 measurements of  $\delta\text{D}$  is  $\pm 3\text{‰}$ , and the accuracy is  $\pm 6.5\text{‰}$ .  
158  
159



160

161 **Figure 1.** Selected flight tracks (red lines) of the NASA P-3B Orion aircraft during the  
 162 ORACLES 2016 IOP used in this study, with corresponding flight dates listed in Table 1.

163 ~~Superimposed on the map are the September 2016 monthly mean 700-hPa winds (white~~  
 164 ~~vectors) and surface pressure (white isobars), along with the approximate biomass~~  
 165 ~~burning region (green rectangle).~~

**Deleted:**

**Deleted:** Also shown is the biomass burning region (green rectangle), 700 hPa winds (white vectors), and surface pressure (white isobars).

167 **Table 1.** Summary of matches of AIRS and WISPER  $\delta D$  measurements during NASA ORACLES\*.

Flight Date	Daily Number of Matched Profiles, loose lat/lon constraint.	Daily Number of Matched Profiles, tighter lat/lon constraint.
31-Aug-2016	138	26
2 Sep 2016	15	15
4 Sep 2016	102	26
10 Sep 2016	48	7
12 Sep 2016	18	4
14 Sep 2016	12	5
20 Sep 2016	11	4
25 Sep 2016	102	23
<b>Total</b>	<b>446</b>	<b>110</b>

168 \*NASA ORACLES is the “ObseRvations of Aerosols above Clouds and their intEractionS” Earth Venture  
 169 Suborbital Mission.  
 170

### 171 3 Satellite Retrieval

#### 172 3.1 Retrieval algorithm

**Deleted: A**

173 The single footprint AIRS HDO profile data used in this work were produced using the  
 174 retrieval algorithm, named the MUlti-SpEctra, MUlti-SpEcies, MUlti-Sensors (MUSES)



180 algorithm (D. Fu et al., 2013, 2016, 2018, 2019; Worden et al., 2019). The MUSES  
181 algorithm can use radiances from multiple instruments including AIRS and other  
182 instruments (CrIS, TES, OMI, OMPS, TROPOMI, and MLS) to quantify geophysical  
183 observables that affect the corresponding radiance. The AIRS single footprint HDO  
184 profile retrievals have been described by Worden et al. (2019), and have heritage from  
185 the TES algorithm (Worden et al., 2004, 2006, 2007, 2011, 2012, 2013; Bowman et al.  
186 2006, 2002). The Optimal Spectral Sampling (OSS) fast radiative transfer model (Moncet  
187 et al., 2008, 2015) for single footprint AIRS measurements has been integrated into the  
188 MUSES algorithm, in support of the operational data production towards the multi-  
189 decadal record of global HDO profiles. The supplement attached to this paper discusses  
190 the sensitivity of the retrievals to the choice of the forward model. The retrieval uses the  
191 optimal estimation (OE) method to quantify atmospheric HDO and H<sub>2</sub>O (Worden et al.  
192 2006, 2012, 2019). For both AIRS and TES retrievals, height discrimination of the  
193 HDO/H<sub>2</sub>O ratio in the troposphere is provided by spectral resolution of pressure and  
194 temperature broadened absorption features of their corresponding lines (Beer et al.,  
195 2002). The algorithms and spectral microwindows are described by Worden et al. (2019).  
196 Chemical species CH<sub>4</sub>, CO, HDO, and H<sub>2</sub>O are jointly retrieved along with atmospheric  
197 temperature, surface temperature, land emissivity and clouds (Worden et al. 2012). The  
198 retrieval optimizes the ratio of HDO to H<sub>2</sub>O, as opposed to either HDO or H<sub>2</sub>O alone  
199 (Worden et al., 2019, 2012, 2006). AIRS radiances at wavelengths from 8 to 12 μm are  
200 used here, excluding the 9.6 μm ozone band. The parent molecule H<sub>2</sub>O is retrieved at  
201 both 8 and 12 μm, but HDO is retrieved primarily from strong absorption lines in the 8  
202 μm region (particularly in the wavenumber range 1210 to 1270 cm<sup>-1</sup>). Cloud optical

203 depth and cloud top pressure are jointly retrieved with the chemical species, using the  
204 approach described in Kulawik et al. (2006). The cloud-clearing approach (Susskind et  
205 al., 2003), utilized in AIRS operational products up to and including AIRS v6, where  
206 retrievals are reported on the 45 km [Advanced Microwave Sounding Unit \(AMSU\)](#)  
207 footprint, is not utilized here. As described by Worden et al. (2019), retrievals are  
208 performed on single AIRS 13.5-km footprints in order to preserve the Level 1B radiance  
209 noise characteristics (Irion et al., 2018; DeSouza-Machado et al., 2018).

210  
211 For H<sub>2</sub>O, the a priori constraint vectors come from NASA's Goddard Earth Observing  
212 System (GEOS) data assimilation system GEOS version 5.12.4 processing stream  
213 (Rienecker et al., 2008). These are produced by the Global Modeling and Assimilation  
214 Office (GMAO) at the NASA Goddard Space Flight Center (GSFC). The GMAO GEOS-  
215 5.12.4 water mixing ratios are linearly interpolated to the latitudes, longitudes, and  
216 log(pressure) levels of [the](#) satellite retrievals to generate the a priori profiles.

217  
218 For all HDO retrievals, the initial profile of the HDO/H<sub>2</sub><sup>16</sup>O isotopic ratio is set equal to a  
219 simulated tropical profile (Worden et al., 2006). In the AIRS HDO product files, a priori  
220 HDO is defined as the product of the local a priori H<sub>2</sub>O profile (GMAO GEOS-5.12.4)  
221 and one tropical a priori profile of the HDO/H<sub>2</sub>O isotopic ratio (Worden et al., 2006). The  
222 initial guess profiles for H<sub>2</sub>O are set equal to the a priori.

223

### 224 **3.2 Method of comparison**

225 The AIRS HDO/H<sub>2</sub>O retrievals are matched up in space and time with the aircraft [in situ](#)

Deleted: in situ

227 HDO/H<sub>2</sub>O measurements. A critical aspect of validating satellite retrievals is obtaining  
228 data that span the altitudes where the satellite has sensitivity to HDO/H<sub>2</sub>O. AIRS data are  
229 sensitive to the HDO/H<sub>2</sub>O ratio in the atmosphere from the surface up to approximately  
230 10,000 m altitude. The aircraft samples HDO and H<sub>2</sub>O from the surface up to 6000 m  
231 altitude, spanning most of the altitudes where the AIRS data are sensitive and therefore  
232 allowing us to validate AIRS HDO/H<sub>2</sub>O with *in situ* measurements.

Deleted: in situ

234 For direct comparison of AIRS HDO/H<sub>2</sub>O with *in situ* HDO/H<sub>2</sub>O, the AIRS instrument  
235 operator (averaging kernel and *a priori* constraint) is applied to the *in situ* data (see Eq. 1  
236 below), as described by Rodgers (2000). This has the effect of smoothing the *in situ* data  
237 to the same resolution as the satellite retrievals. The averaging kernel matrix  $A$  is the  
238 sensitivity of the AIRS estimate to the true concentration in the atmosphere (Rodgers,  
239 2000). The *in situ* profile with applied averaging kernel  $x_{insituw/AK}$  is calculated jointly for  
240 HDO and H<sub>2</sub>O using the AIRS operator:

Deleted: in situ

Deleted: in situ

Deleted: in situ

Deleted: in situ

$$x_{insituw/AK} = x_a + A_{xx}(x - x_a) \quad (1)$$

243 Joint HDO/H<sub>2</sub>O retrievals are performed on the logarithm of the volume mixing ratios,  $x_D$   
244 =  $\ln(q_D)$  and  $x_H = \ln(q_H)$  (Worden et al., 2012, 2006). The data structure for AIRS HDO  
245 files is similar to TES HDO, with details provided by Herman et al. (2014).

247 For comparison with AIRS, the *in situ* HDO and H<sub>2</sub>O profiles are extended to cover the  
248 full range of AIRS levels. In the boundary layer, from the surface up to the lowest  
249 altitude aircraft data, we assume constant values of HDO and H<sub>2</sub>O set equal to the first

Deleted: in situ

256 aircraft measurement. In the range of aircraft data (up to 6000-m flight ceiling), the  
257 aircraft *in situ* HDO and H<sub>2</sub>O data are interpolated to the levels of the AIRS forward  
258 model, smoothing fine scale features. In the layers above the aircraft maximum altitude,  
259 the profile is extrapolated using a scaled a priori profile. In this paper, all comparisons  
260 have been completed *by* applying Eq. 1.

Deleted: in situ

261

## 262 **4 Validation**

263 Validating the accuracy of AIRS HDO and H<sub>2</sub>O retrievals is important for studies of the  
264 hydrologic cycle, exchange processes in the troposphere, and climate change.  
265 Comparisons of AIRS and TES over five years (2006-2010) indicate that the retrieval  
266 characteristics of the AIRS HDO/H<sub>2</sub>O measurements have similar vertical resolution and  
267 uncertainty in the middle troposphere but with slightly less sensitivity in the lower  
268 troposphere (Worden et al., 2019). Worden et al. (2019) reported that the calculated  
269 uncertainty of AIRS HDO/H<sub>2</sub>O is ~30 per mil for a tropospheric average between 750  
270 and 350 hPa, with mean bias between TES and AIRS (TES-AIRS) for the HDO/H<sub>2</sub>O  
271 ratio of ~-2.6 per mil and a latitudinal variation of ~7.6 per mil.

272

### 273 **4.1 Comparison of AIRS with aircraft measurements**

Deleted: A

Deleted: M

#### 274 **ORACLES 8/31 to 9/25/2016 data comparison.**

275 In this section, we describe comparisons between AIRS and ORACLES aircraft HDO  
276 measurements. First, time segments of each aircraft flight are identified where the aircraft  
277 profiled from the boundary layer up to approximately 6000 m altitude. To minimize the  
278 impact of atmospheric spatial and temporal variability, same-day AIRS measurements are

282 selected for the same latitude/longitude rectangle as each aircraft profile (Fig. 2). These  
283 matched pairs are compared by the method described in Sect. 3.2. The loose constraint  
284 (Table 1 column 1, Fig. 2 and Fig. 4a) is that, for an aircraft vertical profile (~ 100 to 300  
285 km in length), all AIRS geolocations within the same rectangle of maximum to minimum  
286 latitude and maximum to minimum longitude are selected. The only exceptions were the  
287 aircraft flights of 9/2/2016 and 9/14/2016, which had different flight patterns and smaller  
288 shapes were used to constrain AIRS geolocations. The tighter constraint (Table 1 column  
289 2, Fig. 2 closed circles and Fig. 4b) is to match only AIRS geolocations within 0.3  
290 degrees (30 km) of the aircraft flight track. The standard data retrieval quality flags for  
291 the retrieval are used in this analysis, which are based on the Aura TES data retrieval  
292 quality flags (Herman and Kulawik, 2018). For closer spatial coincidence, we also  
293 selected AIRS-aircraft measurement pairs within 0.3 degrees (Fig. 2). Following Worden  
294 et al. (2007) and Brown et al. (2008), we filter data for a reasonable threshold of standard  
295 nadir data product DegreesOfFreedomForSignal (DOFS) > 1.1, but include all values of  
296 AverageCloudEffOpticalDepth. Data product DOFS is the trace of the averaging kernel,  
297 and is a measure of the number of independent parameters for the retrieved HDO/H<sub>2</sub>O  
298 profile. AverageCloudEffOpticalDepth is the retrieved cloud mean optical depth at  
299 wavenumbers from 975 to 1200 cm<sup>-1</sup> from the final retrieval step (e.g., the same for all  
300 species) (Kulawik et al., 2006), Fig. 3(a) shows a representative 31 Aug 2016 comparison  
301 between aircraft water vapor δD from WISPER and the coincident AIRS retrieval. Fig.  
302 3(b) shows the corresponding averaging kernels.

**Deleted:** Within each flight are several profiles each spanning 1 to 3 degrees (or ~ 100 to 300 km), so measurement pairs are typically within 3 degrees (Fig. 2).

**Deleted:** 3

**Deleted:** )

**Formatted:** Subscript

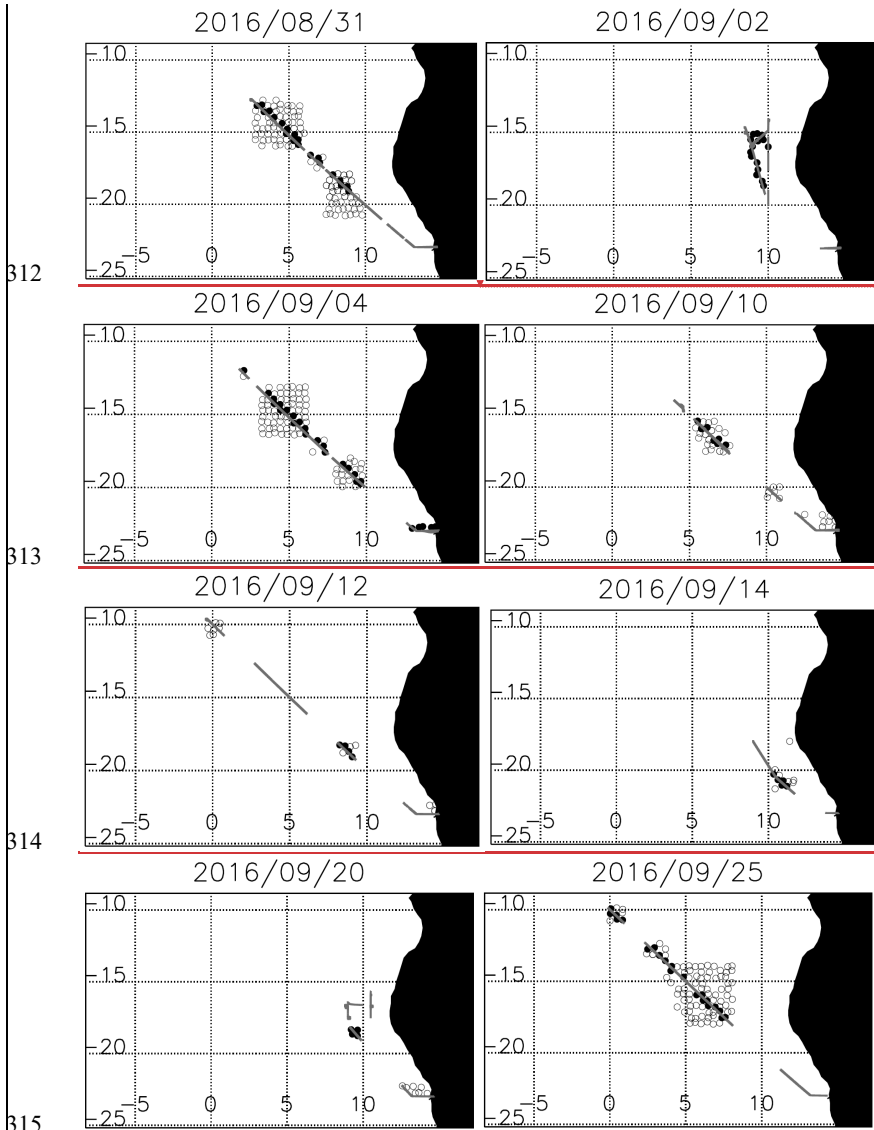
**Formatted:** Superscript

**Deleted:** s

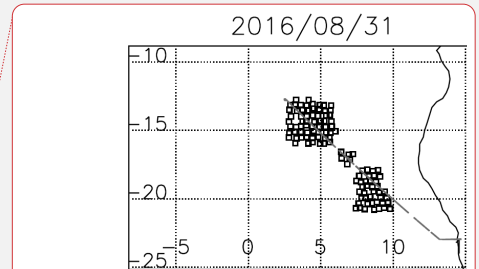
**Deleted:** 4

**Deleted:** 4

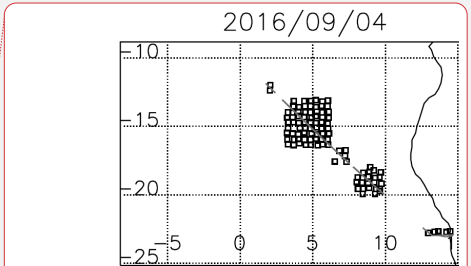
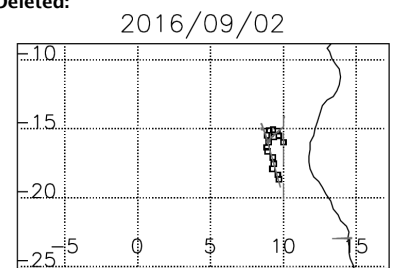
303



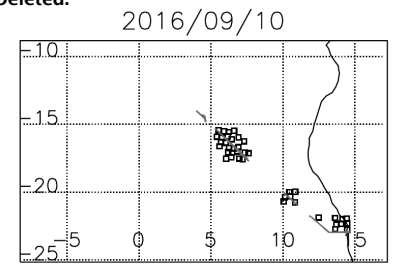
312  
313  
314  
315  
316 **Figure 2.** ORACLES aircraft profiles (thin grey line segments) over the southeast  
317 Atlantic Ocean to the west of Africa are matched to AIRS fields of view (FOVs) in loose  
318 spatial match (open circles) and tight spatial match within 30 km (closed circles) for eight



Deleted:



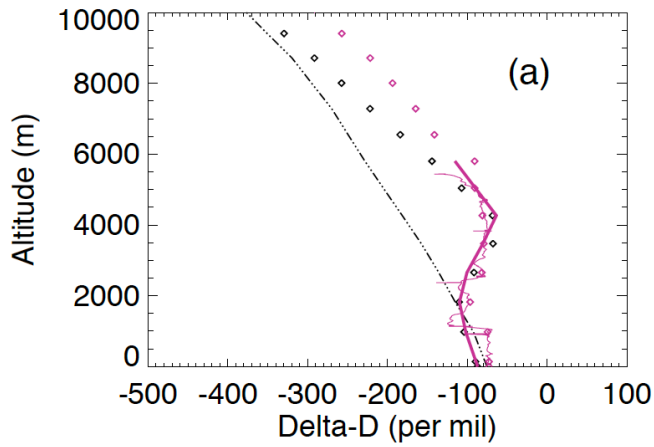
Deleted:



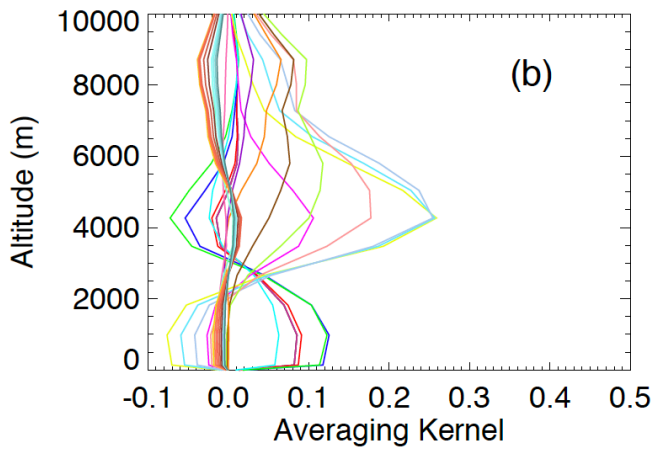
Deleted: (square symbols) within the same latitude/longitude rectangle as the aircraft profiles

330 flights in 2016.

331



332



333

334 **Figure 3.** (a) Sample comparison of the  $\delta D$  profiles by aircraft and satellite over the  
335 southeast Atlantic Ocean during ORACLES on 31 August 2016: shown are AIRS  $\delta D$   
336 (black diamond symbols), the prior  $\delta D$  (black dash-dot-dot line), nearest WISPER  $\delta D$

2016/08/31

Deleted: ... [2]

Deleted: 4

346 (thin red line), WISPER  $\delta D$  interpolated to satellite levels (red diamonds), and the  
347 WISPER  $\delta D$  with the AIRS averaging kernel applied (thick red line).  
348 **(b)** Averaging Kernel corresponding to same AIRS profile on 31 August 2016, color-  
349 coded by pressure level. Averaging kernels with the largest positive sensitivity below  
350 2000 m are from the lowest altitudes.

351

#### 352 **4.2 AIRS bias correction**

353 TES HDO/H<sub>2</sub>O ratios are biased compared to model and *in situ* measurements (Worden  
354 et al., 2006, 2007, 2011). We assess whether AIRS HDO has a bias relative to *in situ*  
355 measurements. As described above, AIRS and TES show a small bias for the HDO/H<sub>2</sub>O  
356 ratio of  $\sim -2.3$  per mil (Worden et al., 2019) after a bias correction is applied, so it is  
357 reasonable to see how well *in situ* and AIRS data agree if the TES bias correction is  
358 applied to the AIRS HDO. Herman et al. (2014) estimated the TES bias  $\delta_{bias}$  by  
359 minimizing the difference between bias-corrected TES and *in situ*  $\delta D$  with TES operator  
360 applied:

$$361 \quad \delta_{bias} = 0.00019 \times Pressure - 0.067 \quad (2)$$

362 We apply the TES  $\delta_{bias}$  to the AIRS data to evaluate against ORACLES aircraft data.

363 There are 446 matched profiles of AIRS and ORACLES within the same

364 latitude/longitude boxes, and 110 closely-matched profiles within 0.3 degrees or  
365 approximately 30 km (Fig. 2). Comparisons with averaging kernel applied are shown in  
366 Fig. 4 and Table 2. Over the range of aircraft data, 0 km to 6 km altitude, AIRS  $\delta D$  has a  
367 mean bias of  $-6.7\%$  relative to the aircraft profiles, well within the estimated  
368 measurement uncertainty of both AIRS and the WISPER calibration. This is consistent

Deleted: B

Deleted: in situ

Deleted: in situ

Deleted: in situ

Deleted: in situ

Deleted: (Fig. 2),

Deleted: 3

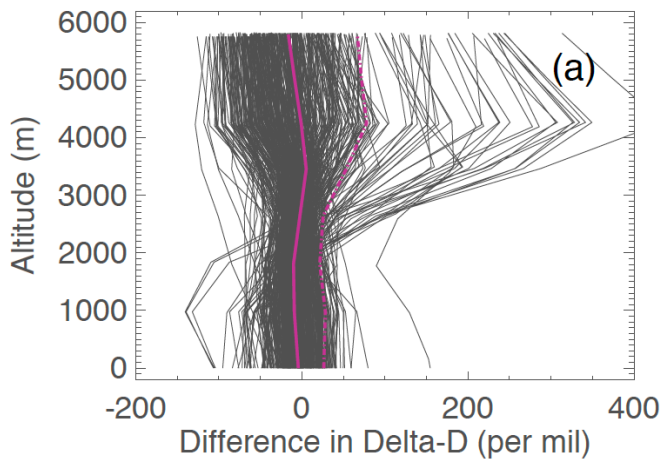
Deleted: 5



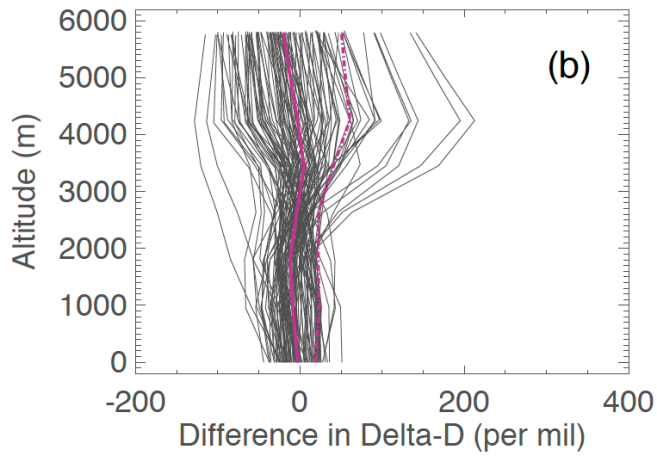
377 with TES  $\delta D$  (Worden et al., 2019; Herman et al., 2014). AIRS lower-tropospheric  $\delta D$   
378 bias is -6.6‰ and RMS 20.9‰ (surface to 800 hPa). In the mid-troposphere, 800 to 500  
379 hPa, AIRS  $\delta D$  bias is -6.8‰ and RMS 44.9‰.

380

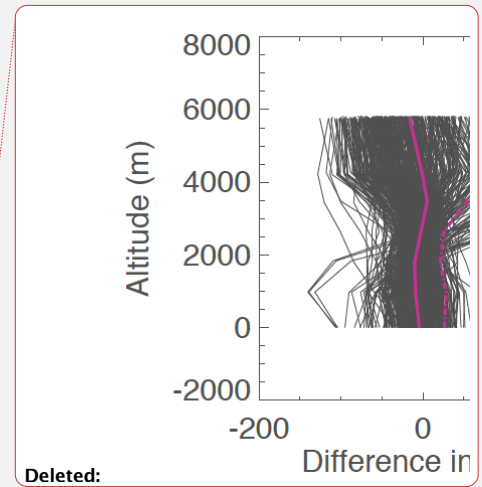
382



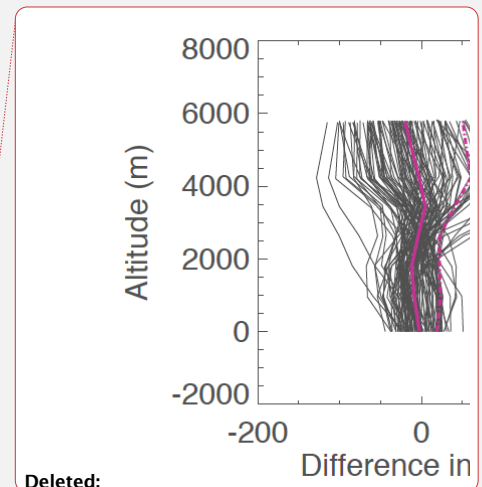
381



383



Deleted:



Deleted:

386 **Figure 4. (a)** AIRS minus ORACLES aircraft  $\delta D$  for the 446 matches within the loose  
 387 spatial matching constraint (Fig. 2 open circles). Lines are individual profiles (black  
 388 lines), mean (red solid line) and RMS (red dash dot line).

Deleted: 5

Deleted: 3 degrees

389 **(b)** AIRS minus ORACLES aircraft  $\delta D$  for the 110 matches within 0.3 degrees (Fig. 2  
 390 closed circles).

Deleted: 3

392 **Table 2.** Summary of satellite-aircraft comparisons for 110 matched pairs in 2016 (Fig. 2 closed circles).

Deleted: 3

393 Bias and RMS (standard deviation) of AIRS  $\delta D$  relative to ORACLE aircraft with averaging kernel applied  
 394 (“BiasAK”, “RMSak”), and for AIRS relative to mapped ORACLES aircraft, no averaging kernel (“Bias”,  
 395 “RMS”). The reported RMS here is the standard deviation, not including the bias.

Altitude (m)	Pressure (hPa)	BiasAK (‰)	RMSak (‰)	Bias (‰)	RMS (‰)
0.01	1014.63	-2.46	18.98	-14.82	22.64
136.61	1000.00	-3.35	19.38	-18.14	22.79
968.87	908.51	-8.86	23.39	-0.31	131.50
1807.71	825.40	-11.80	22.05	9.77	89.68
2641.34	749.89	-3.89	22.63	-13.24	38.07
3456.36	681.29	4.89	41.03	-3.66	35.98
4250.29	618.97	-2.96	60.63	12.52	76.03
5027.62	562.34	-11.87	55.15	-16.62	73.75
5792.12	510.90	-20.09	50.61	-40.41	81.22

396

397

## 398 5. Error estimation

399 In this section we characterize the *a posteriori* error budget for AIRS HDO/H<sub>2</sub>O and  
 400 assess this error by comparison with the ORACLES aircraft measurements. Error analysis  
 401 in OE has been described in detail in the literature (Worden et al., 2004, 2006; Bowman

Formatted: Font: Italic

Formatted: Subscript

Deleted: optimal estimation

407 et al., 2004; Rodgers, 2000). The error  $\mathbf{x}$  in the estimate of HDO/H<sub>2</sub>O is defined as the  
 408 true state  $\mathbf{x}$  minus the linear estimate  $\hat{\mathbf{x}}$  retrieved by AIRS (e.g., Worden et al., 2006, Eq.  
 409 (15)):

$$410 \quad \mathbf{x} = \mathbf{x} - \hat{\mathbf{x}}. \quad (3)$$

411 Similar to Herman et al. (2014), we define the *estimated error* of the AIRS isotopic ratio  
 412 HDO/H<sub>2</sub>O, (Eq. 4) as the observation error covariance (Worden et al., 2006):

$$413 \quad \mathbf{S} = \mathbf{G}_R \mathbf{S}_n \mathbf{G}_R^T + \mathbf{G}_R \left( \sum_i \mathbf{K}_i \mathbf{S}_b^i \mathbf{K}_i^T \right) \mathbf{G}_R^T, \quad (4)$$

414 where  $\mathbf{G}_R = (\mathbf{G}_z^D - \mathbf{G}_z^H)$  is the gain matrix of the HDO/H<sub>2</sub>O retrieval,  $\mathbf{S}_n$  is the  
 415 measurement error covariance, and  $\mathbf{S}_b^i$  is the error covariance due to systematic errors and  
 416 interference errors. Interference errors are due to CH<sub>4</sub>, N<sub>2</sub>O, surface emissivity, effects of  
 417 temperature, and clouds. The estimated error is given by the square roots of the diagonal  
 418 elements of  $\mathbf{S}$ , the best estimate of the AIRS observation error covariance for the  
 419 HDO/H<sub>2</sub>O retrieval.

421 The estimated error (Eq. 4) is compared to the empirical error calculated from the AIRS-  
 422 aircraft comparisons. It is seen that the error varies from ~20 to ~40 per mil (Fig. 5). The  
 423 empirical error (AIRS versus aircraft RMS) is similar in magnitude to the estimated error,  
 424 but exceeds the estimated error at 500 to 600 hPa in the free troposphere. These  
 425 differences between the OE estimated error and the empirical error are likely due to  
 426 uncertainties in atmospheric variability in space and time and in the collocation between  
 427 satellite retrieval and aircraft measurements. The instrument operator (Eq. 1) accounts for  
 428 error due to the mismatch in \*vertical\* sensitivity between the satellite retrieval and  
 429 aircraft *in situ* vertical profiling. In the cases where AIRS is compared to *in situ*

Formatted: Subscript

Deleted: ,

Formatted: Subscript

Formatted: Subscript

Deleted: In the case where AIRS is compared to in situ measurements without the averaging kernel, there is an additional smoothing error.

Formatted: Line spacing: Double, No widow/orphan control, Don't adjust space between Latin and Asian text, Don't adjust space between Asian text and numbers, Tab stops: 0.5", Left + 1", Left + 1.5", Left + 2", Left + 2.5", Left + 3", Left + 3.5", Left + 4", Left + 4.5", Left + 5", Left + 5.5", Left + 6", Left

Deleted: 6

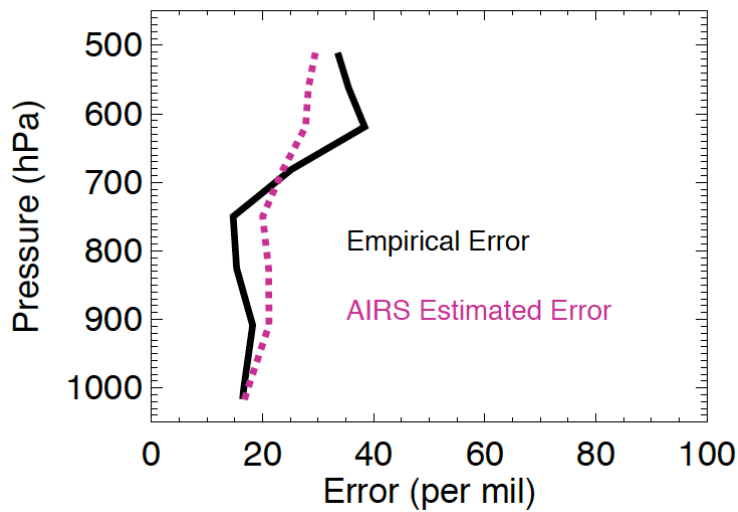
Formatted: Font: Italic

Formatted: Font: Italic

435 measurements without the instrument operator, there is an additional smoothing error  
436 (Table 2). The instrument operator does not account for error due to \*horizontal\*  
437 mismatch. The close coincidences are all within 30 km (0.3 degrees), but given time  
438 differences, and the AIRS 15-km nadir footprint and limited in situ measurement, the  
439 satellite and aircraft are not necessarily measuring the same airmass. There is a  
440 collocation error on the order of ~10 per mil due to horizontal  
441 collocation/representativeness uncertainty.

**Deleted:** These differences are likely due to atmospheric variability as we do not have exact matchups between the AIRS data and aircraft measurements.

445



446

447 **Figure 5.** Plot of AIRS error analysis for coincident AIRS and ORACLES  $\delta D$  on 31  
448 August 2016 shows that the empirical error is comparable to the AIRS estimated error.  
449 The empirical error is obtained from the statistics of the satellite-aircraft comparison,  
450 while the estimated error is obtained from optimal estimation retrieval theory. Plotted  
451 here, are the AIRS  $\delta D$  estimated error also known as AIRS observation error (red dashed  
452 line) and the AIRS  $\delta D$  empirical error (black line).

Deleted: 6

Formatted: Font: Not Bold

Deleted: Plotted

453

454

## 455 6. Conclusions

456 HDO/H<sub>2</sub>O estimates from AIRS single footprint radiances been compared to coincident  
457 in situ airborne measurements on the P-3B Orion aircraft by the Oregon State Water  
458 WISPER system, over the Southeast Atlantic Ocean. On eight days between 31 Aug and

Deleted: in situ

Deleted: (Water Isotope Spectrometer for Precipitation and Entrainment Research)

464 25 Sep 2016, there are collocated measurements between AIRS and the P-3B aircraft. We  
465 have shown that AIRS-only retrievals have sensitivity to HDO from the middle  
466 troposphere to the lower troposphere. We demonstrate that AIRS  $\delta D$  has a mean bias of -  
467 6.7‰ relative to aircraft, well within the estimated measurement uncertainty. In the lower  
468 troposphere, 1000 to 800 hPa, AIRS  $\delta D$  bias is -6.6‰ and the RMS 20.9‰, consistent  
469 with the calculated uncertainty of 19.1‰. In the mid-troposphere, 800 to 500 hPa, AIRS  
470  $\delta D$  bias is -6.8‰ and RMS 44.9‰, comparable to the calculated uncertainty of 25.8‰.  
471 The errors are sufficiently small that the AIRS HDO/H<sub>2</sub>O ratio retrievals are useful for  
472 scientific analysis. This long term global data record has much potential utility.  
473

Deleted: boundary layer

Formatted: Subscript

475 **Code/Data availability.** The ORACLES aircraft data used in the data analysis can be  
476 freely downloaded from the following Digital Object Identifier:  
477 ([http://dx.doi.org/10.5067/Suborbital/ORACLES/P3/2016\\_V1](http://dx.doi.org/10.5067/Suborbital/ORACLES/P3/2016_V1), last access: 22 April  
478 2017). We expect the AIRS-based deuterium data to be publicly released by January  
479 2020. Files in IDL format of the AIRS data shown and forward model output are  
480 available from coauthor John Worden upon request: [john.r.worden@jpl.nasa.gov](mailto:john.r.worden@jpl.nasa.gov).

481

482 **Team list.** Robert L. Herman (RH), John Worden (JW), David Noone (DN), Dean  
483 Henze (DH), Kevin Bowman (KB), Karen Cady-Pereira (KC), Vivienne H. Payne (VP),  
484 Susan S. Kulawik (SK), and Dejian Fu (DF).

485

486 **Author contribution.** RH carried out all steps of aircraft validation, from matching data  
487 and quality filtering to applying observation operator and statistics, while JW provided  
488 satellite-to-satellite validation. JW developed the retrieval strategies for both AIRS and  
489 TES HDO/H<sub>2</sub>O retrievals. DF and SK built the strategies of single AIRS footprint  
490 HDO/H<sub>2</sub>O retrievals into the MUSES algorithm. KC, RH and VP evaluated the  
491 sensitivities of retrievals to the choice of forward model. RH, VP, JW, SK, DF, DN, DH  
492 and KB contributed to the text and interpretation of the results. JW and SK helped in the  
493 estimation of HDO/H<sub>2</sub>O measurement uncertainty, quality flagging and knowledge of the  
494 retrieval process. DN and DH provided ORACLES data, aircraft measurement  
495 uncertainty, and identified profiles in the aircraft data. All authors participated in writing  
496 the manuscript.

497

498 **Competing interests.** The authors declare that they have no conflict of interest.

499

500 **Acknowledgments**

501 Support for R. Herman, J. Worden, S. Kulawik, D. Fu and V. Payne was provided by the  
502 NASA Aura Program. Participation by D. Noone and D. Henze was supported by a grant  
503 from the National Science Foundation Climate and Large-scale Dynamics, and  
504 Atmospheric Chemistry programs (AGS 1564670). Part of the research described in this  
505 paper was carried out by the Jet Propulsion Laboratory, California Institute of  
506 Technology, under a contract with NASA.

507



508 **References**

- 509 Aumann, H. H., Chahine, M. T., Gautier, C., Goldberg, M. D., Kalnay, E., McMillin, L.  
510 M., Revercomb, H., Rosenkranz, P. W., Smith, W. L., Staelin, D. H., Strow, L. L.,  
511 and Susskind, J.: AIRS/AMSU/HSB on the aqua mission: Design, science objectives,  
512 data products, and processing systems. *IEEE Transactions on Geoscience and Remote*  
513 *Sensing*, 41(2), 253-264, 2003.
- 514 Bailey, A., Blossey, P. N., Noone, D., Nusbaumer, J. & Wood, R. Detecting shifts in  
515 tropical moisture imbalances with satellite-derived isotope ratios in water vapor.  
516 *Journal of Geophysical Research-Atmospheres* **122**, 5763–5779 (2017).
- 517 Beer, R.: TES on the Aura Mission: scientific objectives, measurements and analysis  
518 overview, *IEEE T. Geosci. Remote*, 44, 1102-1105, 2006.
- 519 Beer, R., Bowman, K. W., Brown, P. D., Clough, S. A., Eldering, A., Goldman, A.,  
520 Jacob, D. J., Lampel, M., Logan, J. A., Luo, M., Murcray, F. J., Osterman, G. B.,  
521 Rider, D. M., Rinsland, C. P., Rodgers, C. D., Sander, S. P., Shephard, M., Sund, S.,  
522 Ustinov, E. A., Worden, H. M., Worden, J., and Syvertson, M. (Eds.): Tropospheric  
523 Emission Spectrometer (TES) Level 2 Algorithm Theoretical Basis Document, V.  
524 1.16, Jet Propulsion Laboratory, Pasadena, CA, JPL D-16474, 27 June 2002,  
525 available at <http://eosps.gsfc.nasa.gov/atbd-category/53> (last access: 7 December  
526 2010), 2002.
- 527 Beer, R., Glavich, T. A., and Rider, D. M.: Tropospheric emission spectrometer for the  
528 Earth Observing System's Aura satellite, *Appl. Optics*, 40, 2356-2367, 2001.
- 529 Berden, G., Peeters, R., and Meijer, G.: Cavity ring-down spectroscopy: Experimental  
530 schemes and applications, *Int. Rev. Phys. Chem.*, 19, 565-607, doi:

531 10.1080/014423500750040627, 2000.

532 Berkelhammer, M., Hu, J., Bailey, A., Noone, D., Still, C., Barnard, H., Gochis, D.,  
533 Hsiao, G., Rahn, T., and Turnipseed, A.: The nocturnal water cycle in an open-  
534 canopy forest, *J. Geophys. Res.-Atmos.*, 118, 10225-10242, doi:10.1002/jgrd.50701,  
535 2013.

536 Bernath, P. F., McElroy, C. T., Abrams, M. C., Boone, C. D., Butler, M., Camy-Peyret,  
537 C., Carleer, M., Clerbaux, C., Coheur, P.-F., Colin, R., DeCola, P., DeMazière, M.,  
538 Drummond, J. R., Dufour, D., Evans, W. F. J., Fast, H., Fussen, D., Gilbert, K.,  
539 Jennings, D. E., Llewellyn, E. J., Lowe, R. P., Mahieu, E., McConnell, J. C.,  
540 McHugh, M., McLeod, S. D., Michaud, R., Midwinter, C., Nassar, R., Nichitiu, F.,  
541 Nowlan, C., Rinsland, C. P., Rochon, Y. J., Rowlands, N., Semeniuk, K., Simon, P.,  
542 Skelton, R., Sloan, J. J., Soucy, M.-A., Strong, K., Tremblay, P., Turnbull, D.,  
543 Walker, K. A., Walkty, I., Wardle, D. A., Wehrle, V., Zander, R., and Zou, J.:  
544 Atmospheric Chemistry Experiment (ACE): Mission overview, *Geophys. Res. Lett.*,  
545 32, L15S01, doi:10.1029/2005GL022386, 2005.

546 Bowman, K. W., Worden, J., Steck, T., Worden, H. M., Clough, S., and Rodgers, C.:  
547 Capturing time and vertical variability of tropospheric ozone: A study using TES  
548 nadir retrievals, *J. Geophys. Res.-Atmos.*, 107, 4723, doi:10.1029/2002JD002150,  
549 2002.

550 Bowman, K. W., Rodgers, C. D., Kulawik, S. S., Worden, J., Sarkissian, E., Osterman,  
551 G., Steck, T., Luo, M., Eldering, A., Shephard, M. W., Worden, H., Lampel, M.,  
552 Clough, S. A., Brown, P., Rinsland, C., Gunson, M., and Beer, R.: Tropospheric  
553 Emission Spectrometer: retrieval method and error analysis, *IEEE T. Geosci. Remote*,

554 44, 1297-1307, 2006.

555 Boxe, C. S., Worden, J. R., Bowman, K. W., Kulawik, S. S., Neu, J. L., Ford, W. C.,  
556 Osterman, G. B., Herman, R. L., Eldering, A., Tarasick, D. W., Thompson, A. M.,  
557 Doughty, D. C., Hoffmann, M. R., and Oltmans, S. J.: Validation of northern latitude  
558 Tropospheric Emission Spectrometer stare ozone profiles with ARC-IONS sondes  
559 during ARCTAS: sensitivity, bias and error analysis, *Atmospheric Chemistry and  
560 Physics*, doi:10.5194/acp-10-9901-2010, 2010.

561 Brown, D., Worden, J., and Noone, D.: Comparison of atmospheric hydrology over  
562 convective continental regions using water vapor isotope measurements from space,  
563 *J. Geophys. Res.*, 113, D15124, doi:10.1029/2007JD009676, 2008.

564 Craig, H.: Isotopic Variations in Meteoric Waters, *Science*, 133, 1702-3, doi:  
565 10.1126/science.133.3465.1702, 1961.

566 Dansgaard, W.: Stable isotopes in precipitation, *Tellus*, 16, 436-68, 1964.

567 DeSouza-Machado, S., Strow, L. L., Tangborn, A., Huang, X., Chen, X., Liu, X., Wu, W.  
568 and Yang, Q.: Single-footprint retrievals for AIRS using a fast TwoSlab cloud-  
569 representation model and the SARTA all-sky infrared radiative transfer algorithm,  
570 *Atmos. Meas. Tech.*, 11(1), 529–550, doi:10.1029/2005GL023211, 2018.

571 Frankenberg, C., Yoshimura, K., Warneke, T., Aben, I., Butz, A., Deutscher, N., Griffith,  
572 D., Hase, F., Notholt, J., Schneider, M., Schrijver, H., and Röckmann, T.: Dynamic  
573 Processes Governing Lower-Tropospheric HDO/H<sub>2</sub>O Ratios as Observed from Space  
574 and Ground, *Science*, 325, 1374, DOI: 10.1126/science.1173791, 2009.

575 Fu, D., Bowman, K. W., Worden, H. M., Natraj, V., Worden, J. R., Yu, S., Veefkind, P.,  
576 Aben, I., Landgraf, J., Strow, L., and Han, Y.: High-resolution tropospheric carbon

Moved (insertion) [1]

577 [monoxide profiles retrieved from CrIS and TROPOMI, Atmos. Meas. Tech., 9, 2567-](#)  
578 [2579, https://doi.org/10.5194/amt-9-2567-2016, 2016.](#)

579 Fu, D., Kulawik, S. S., Miyazaki, K., Bowman, K. W., Worden, J. R., Eldering, A.,  
580 Livesey, N. J., Teixeira, J., Irion, F. W., Herman, R. L., Osterman, G. B., Liu, X.,  
581 Levelt, P. F., Thompson, A. M., and Luo, M.: Retrievals of tropospheric ozone  
582 profiles from the synergism of AIRS and OMI: methodology and validation, Atmos.  
583 Meas. Tech., 11, 5587-5605, [https://doi.org/10.5194/amt-11-5587-2018](#), 2018.

584 [Fu, D., Millet, D. B., Wells, K. C., Payne, V. H., Yu, S., Guenther, A., and Eldering, A.:](#)  
585 [Direct retrieval of isoprene from satellite-based infrared measurements, Nature](#)  
586 [Communication, 10.3811, doi:10.1038/s41467-019-11835-0, 2019.](#)

587 Fu, D., Worden, J. R., Liu, X., Kulawik, S. S., Bowman, K. W., and Natraj, V.:  
588 Characterization of ozone profiles derived from Aura TES and OMI radiances,  
589 Atmos. Chem. Phys., 13, 3445-3462, [https://doi.org/10.5194/acp-13-3445-2013](#),  
590 2013.

591 Fu, R.: *et al.* Increased dry-season length over southern Amazonia in recent decades and  
592 its implication for future climate projection. *Proceedings of the National Academy of*  
593 *Sciences of the United States of America* **110**, 18110–18115 (2013).

594 Galewsky, J., Steen-Larsen, H.-C., Field, R. D., Worden, J., Risi, C., and Schneider, M.:  
595 [Stable isotopes in atmospheric water vapor and applications to the hydrologic cycle,](#)  
596 *Rev. Geophys.*, 54, 4, 809-65, 2016.

597 Good, S. P., Noone, D., Bowen, G., Hydrologic connectivity constrains partitioning of  
598 global terrestrial water fluxes, *Science*, 349, 6244, 175-177, 2015.

599 Gupta, P., Noone, D., Galewsky, J., Sweeny, C., and Vaughn, B. H.: Demonstration of

**Moved up [1]:** Fu, D., Bowman, K. W., Worden, H. M., Natraj, V., Worden, J. R., Yu, S., Veeckind, P., Aben, I., Landgraf, J., Strow, L., and Han, Y.: High-resolution tropospheric carbon monoxide profiles retrieved from CrIS and TROPOMI, Atmos. Meas. Tech., 9, 2567-2579, [https://doi.org/10.5194/amt-9-2567-2016](#), 2016.¶

**Deleted:** Stable isotopes in atmospheric water vapor and applications to the hydrologic cycle,

**Formatted:** Default Paragraph Font

**Formatted:** Default Paragraph Font

608 high precision continuous measurements of water vapor isotopologues in laboratory  
609 and remote field deployments using WS-CRDS technology, *Rapid Commun. Mass*  
610 *Sp.*, 23, 2534-2542, doi: 10.1002/rcm.4100, 2009.

611 [Henze, D., and Noone, D.: The Dependence of Entrainment and Drizzle in Marine](#)  
612 [Stratiform Clouds on Biomass Burning Aerosols Derived from Stable Isotope and](#)  
613 [Thermodynamic Profiles, AGU Fall Meeting, New Orleans, Louisiana, United States,](#)  
614 [Abstract A11C-0048, 2017.](#)

615 Henze, D., Toohey, D., and Noone, D.: The Water Isotope Spectrometer for Precipitation  
616 and Entrainment Research (WISPER), in prep., 2019.

617 Herbin, H., Hurtmans, D., Turquety, S., Wespes, C., Barret, B., Hadji-Lazaro, J., Clerbaux,  
618 C., and Coheur, P.-F.: Global distributions of water vapour isotopologues retrieved  
619 from IMG/ADEOS data, *Atmos. Chem. Phys.*, 7, 3957–3968, doi:10.5194/acp-7-3957-  
620 2007, 2007.

621 Herbin, H., Hurtmans, D., Clerbaux, C., Clarisse, L., and Coheur, P.-F.: H<sub>2</sub><sup>16</sup>O and HDO  
622 measurements with IASI/MetOp, *Atmos. Chem. Phys.*, 9, 9433-9447,  
623 doi:10.5194/acp-9-9433-2009, 2009.

624 Herman, R. L., Cherry, J. E., Young, J., Welker, J. M., Noone, D., Kulawik, S. S., and  
625 Worden, J.: Aircraft validation of Aura Tropospheric Emission Spectrometer retrievals  
626 of HDO/H<sub>2</sub>O, *Atmos. Meas. Tech.*, 7, 3127–3138, 2014, 2014.

627 Herman, R. L., and Kulawik, S. S. (Eds.): Tropospheric Emission Spectrometer TES Level  
628 2 (L2) Data User’s Guide, D-38042, version 7.0, Jet Propulsion Laboratory, California  
629 Institute of Technology, Pasadena, CA, available at:

630 [https://eosweb.larc.nasa.gov/project/tes/guide/TESDataUsersGuideV7\\_0\\_Sep\\_27\\_20](https://eosweb.larc.nasa.gov/project/tes/guide/TESDataUsersGuideV7_0_Sep_27_2018_FV-2.pdf)  
631 [18\\_FV-2.pdf](https://eosweb.larc.nasa.gov/project/tes/guide/TESDataUsersGuideV7_0_Sep_27_2018_FV-2.pdf) (last access: 18 October 2018), 2018.

632 Herman, R. L., and Osterman, G. B. (Eds.): Tropospheric Emission Spectrometer Data  
633 Validation Report (Version F08\_11 data), D-33192, Version 7.0, Jet Propulsion  
634 Laboratory, California Institute of Technology, Pasadena, CA, available at:  
635 [https://eosweb.larc.nasa.gov/sites/default/files/project/tes/readme/TES\\_Validation\\_Re](https://eosweb.larc.nasa.gov/sites/default/files/project/tes/readme/TES_Validation_Report_v7_Final.pdf)  
636 [port\\_v7\\_Final.pdf](https://eosweb.larc.nasa.gov/sites/default/files/project/tes/readme/TES_Validation_Report_v7_Final.pdf) (last access: 15 October 2018), 2018.

637 Irion, F. W., Kahn, B. H., Schreier, M. M., Fetzer, E. J., Fishbein, E., Fu, D., Kalmus, P.,  
638 Wilson, R. C., Wong, S. and Yue, Q.: Single-footprint retrievals of temperature,  
639 water vapor and cloud properties from AIRS, *Atmos. Meas. Tech.*, 11(2), 971–995,  
640 doi:10.1117/12.615244, 2018.

641 Irion, F. W., Moyer, E. J., Gunson, M. R., Rinsland, C. P., Yung, Y. L., Michelsen, H. A.,  
642 Salawitch, R. J., Chang, A. Y., Newchurch, M. J., Abbas, M. M., Abrams, M. C., and  
643 Zander, R.: Stratospheric observations of CH<sub>3</sub>D and HDO from ATMOS infrared  
644 solar spectra: Enrichments of deuterium in methane and implications for HD,  
645 *Geophys. Res. Lett.*, 23(17), 2381–4, 1996.

646 Kuang, Z., Toon, G. C., Wennberg, P. O., and Yung, Y. L.: Measured HDO/H<sub>2</sub>O ratios  
647 across the tropical tropopause, *Geophys. Res. Lett.*, 30(7), 1372,  
648 doi:10.1029/2003GL017023, 2003.

649 Kulawik, S. S., Bowman, K. W., Luo, M., Rodgers, C. D., and Jourdain, L.: Impact of  
650 nonlinearity on changing the a priori of trace gas profile estimates from the  
651 Tropospheric Emission Spectrometer (TES), *Atmos. Chem. Phys.*, 8, 3081–92,  
652 doi:10.5194/acp-8-3081-2008, 2008.

653 Kulawik, S. S., Worden, H., Osterman, G., Luo, M., Beer, R., Worden, J., Bowman, K.,  
654 Eldering, A., Lampel, M., Steck, T., and Rodgers, C.: TES Atmospheric Profile  
655 Retrieval Characterization: An orbit of simulated observations, IEEE T. Geosci.  
656 Remote, 44, 1324-1333, 2006.

657 Kulawik, S. S., Worden, J., Eldering, A., Bowman, K., Gunson, M., Osterman, G. B.,  
658 Zhang, L., Clough, S., Shephard, M. W. and Beer, R.: Implementation of cloud  
659 retrievals for Tropospheric Emission Spectrometer (TES) atmospheric retrievals: part  
660 1. Description and characterization of errors on trace gas retrievals, J. Geophys. Res.,  
661 111, D24204, doi:10.1029/2005JD006733, 2006.

662 Lacour, J.-L., Risi, C., Clarisse, L., Bony, S., Hurtmans, D., Clerbaux, C., and Coheur,  
663 P.-F.: Mid-tropospheric  $\delta D$  observations from IASI/MetOp at high spatial and  
664 temporal resolution, Atmos. Chem. Phys., 12, 10817–10832, doi:10.5194/acp-12-  
665 10817-2012, 2012.

666 Lee, J., Worden, J., Noone, D., Bowman, K., Eldering, A., LeGrande, A., Li, J. L. F.,  
667 Schmidt, G., and Sodemann, H.: Relating tropical ocean clouds to moist processes  
668 using water vapor isotope measurements, Atmos. Chem. Phys., 11, 741-752,  
669 doi:10.5194/acp-11-741-2011, 2011.

670 Lossow, S., Steinwagner, J., Urban, J., Dupuy, E., Boone, C. D., Kellmann, S., Linden,  
671 A., Kiefer, M., Grabowski, U., Glatthor, N., Hopfner, M., Rockmann, T., Murtagh, D.  
672 P., Walker, K. A., Bernath, P. F., von Clarmann, T., and Stiller, G. P.: Comparison of  
673 HDO measurements from Envisat/MIPAS with observations by Odin/SMR and  
674 SCISAT/ACE-FTS, Atmos. Meas. Tech., 4, 1855-1874, doi:10.5194/amt-4-1855-  
675 2011, 2011.

Deleted: ¶

Formatted: Indent: Left: 0", Hanging: 0.25", No bullets or numbering

677 Moncet, J.-L., Uymin, G., Liang, P., and Lipton, A. E.: Fast and accurate radiative  
678 transfer in the thermal regime by simultaneous optimal spectral sampling over all  
679 channels, *J. Atmos. Sci.*, 72, 2622–2641, <https://doi.org/10.1175/JAS-D-14-0190.1>,  
680 2015.

681 Moncet, J.-L., Uymin, G., Lipton, A. E., and Snell, H. E.: Infrared radiance modeling by  
682 optimal spectral sampling, *J. Atmos. Sci.*, 65, 3917–3934,  
683 <https://doi.org/10.1175/2008JAS2711.1>, 2008.

684 Moyer, E. J., Irion, F. W., Yung, Y. L., and Gunson, M. R.: ATMOS stratospheric  
685 deuterated water and implications for troposphere-stratosphere transport, *Geophys.*  
686 *Res. Lett.*, 23(17), 2385-8, 1996.

687 Murtagh, D., Frisk, U., Merino, F., Ridal, M., Jonsson, A., Stegman, J., Witt, G.,  
688 Eriksson, P., Jiménez, C., Megie, G., de la Noë, J., Ricaud, P., Baron, P., Pardo, J. R.,  
689 Hauchcorne, A., Llewellyn, E. J., Degenstein, D. A., Gattinger, R. L., Lloyd, N. D.,  
690 Evans, W. F. J., McDade, I. C., Haley, C. S., Sioris, C., von Savigny, C., Solheim, B.  
691 H., McConnell, J. C., Strong, K., Richardson, E. H., Leppelmeier, G. W., Kyrölä, E.,  
692 Auvinen, H., and Oikarinen, L.: An overview of the Odin atmospheric mission, *Can.*  
693 *J. Phys.*, 80, 309-319, doi:10.1139/p01-157, 2002.

694 [Nassar, R., Bernath, P. F., Boone, C. D., Gettelman, A., McLeod, S. D., and Rinsland, C.](#)  
695 [P.: Variability in HDO/H<sub>2</sub>O abundance ratios in the tropical tropopause layer, \*J.\*](#)  
696 [Geophys. Res.](#), 112, D21305, doi:10.1029/2007JD008417, 2007.

697 Noone, D.: Pairing Measurements of the Water Vapor Isotope Ratio with Humidity to  
698 Deduce Atmospheric Moistening and Dehydration in the Tropical Midtroposphere,  
699 *Journal of Climate*, 25(13), 4476-4494, 2012.



700 Noone, D., Galewsky, J., Sharp, Z. D., Worden, J., Barnes, J., Baer, D., Bailey, A.,  
701 Brown, D. P., Christensen, L., Crosson, E., Dong, F., Hurley, J. V., Johnson, L. R.,  
702 Strong, M., Toohey, D., Van Pelt, A., and Wright, J. S.: Properties of air mass mixing  
703 and humidity in the subtropics from measurements of the D/H isotope ratio of water  
704 vapor at the Mauna Loa Observatory, *J. Geophys. Res.-Atmos.*, 116, D22113,  
705 doi:10.1029/2011JD015773, 2011.

706 O’Keefe, A., and Deacon, D. A. G.: Cavity ringdown optical spectrometer for absorption  
707 measurements using pulsed laser sources, *Rev. Sci. Instrum.*, 59, 2544; doi:  
708 10.1063/1.1139895, 1988.

709 ORACLES Science Team: Suite of Aerosol, Cloud, and Related Data Acquired Aboard  
710 P3 During ORACLES 2016, Version 1, NASA Ames Earth Science Project Office,  
711 [http://dx.doi.org/10.5067/Suborbital/ORACLES/P3/2016\\_V1](http://dx.doi.org/10.5067/Suborbital/ORACLES/P3/2016_V1), 2017.

712 Pagano, T. S., Aumann, H. H., Hagan, D. E., and Overoye, K.: Prelaunch and in-flight  
713 radiometric calibration of the Atmospheric Infrared Sounder (AIRS), *IEEE*  
714 *Transactions on Geoscience and Remote Sensing*, 41(2), 265-273, 2003.

715 Pagano, T. S., Aumann, H., Schindler, R., Elliott, D., Broberg, S., Overoye, K., Weiler,  
716 M.: Absolute Radiometric Calibration Accuracy of the Atmospheric Infrared  
717 Sounder, *Proc SPIE*, 7081-46, San Diego, California, August, 2008.

718 Pougatchev, N., August, T., Calbet, X., Hultberg, T., Oduleye, O., Schlüssel, P., Stiller,  
719 B., St. Germain, K., and Bingham, G.: IASI temperature and water vapor retrievals –  
720 error assessment and validation, *Atmos. Chem. Phys.*, 9, 6453-6458, doi:10.5194/acp-  
721 9-6453-2009, 2009.

722 Randel, W. J., Moyer, E., Park, M., Jensen, E., Bernath, P., Walker, K., and Boone, C.:

723 Global variations of HDO and HDO/H<sub>2</sub>O ratios in the upper troposphere and lower  
724 stratosphere derived from ACE-FTS satellite measurements, *J. Geophys. Res.-*  
725 *Atmos.*, 117, D06303, doi:10.1029/2011JD016632, 2012.

726 Rienecker, M. M., Suarez, M. J., Todling, R., Bacmeister, J., Takacs, L., Liu, H.-C., Gu,  
727 W., Sienkiewicz, M., Koster, R. D., Gelaro, R., and Stajner, I., and Nielson, J. E.: The  
728 GEOS-5 Data Assimilation System: Documentation of Versions 5.0, 5.1.0 and 5.2.0,  
729 NASA TM 104606, 27, NASA Technical Report Series on Global Modeling and Data  
730 Assimilation, 2008.

731 Rinsland, C. P., Gunson, M. R., Foster, J. C., Toth, R. A., Farmer, C. B., and Zander, R.:  
732 Stratospheric Profiles of Heavy Water Vapor Isotopes and CH<sub>3</sub>D From Analysis of  
733 the ATMOS Spacelab 3 Infrared Solar Spectra, *J. Geophys. Res.*, 96, 1057-1068,  
734 1991.

735 Rodgers, C. D.: *Inverse Methods for Atmospheric Sounding: Theory and Practice*, World  
736 Science, London, 2000.

737 Rodgers, C. D., and Connor, B. J.: Intercomparison of Remote Sounding Instruments, *J.*  
738 *Geophys. Res.*, 108, 4116, doi: 10.1029/2002JD002299, 2003.

739 [Schneider, A., Borsdorff, T., Brugh, J., Aemisegger, F., Feist, D., Kivi, R., Hase, F.,](#)  
740 [Schneider, M., and Landgraf, J.: First data set of H<sub>2</sub>O/HDO columns from the](#)  
741 [Tropospheric Monitoring Instrument \(TROPOMI\), \*Atmos. Meas. Tech.\*, 13, 85–100,](#)  
742 <https://doi.org/10.5194/amt-13-85-2020>, 2020.

743 Schneider, M., and Hase, F.: Optimal estimation of tropospheric H<sub>2</sub>O and δD with  
744 IASI/METOP, *Atmos. Chem. Phys.*, 11, 11207-220, doi: 10.5194/acp-11-11207-  
745 2011, 2011.

Formatted: Subscript

746 Schneider, M., Hase, F., and Blumenstock, T.: Ground-based remote sensing of  
747 HDO/H<sub>2</sub>O ratio profiles: Introduction and validation of an innovative retrieval  
748 approach, *Atmos. Chem. Phys.*, 6, 4705–4722, doi:10.5194/acp-6-4705-2006, 2006.

749 Schneider, M., Toon, G., Blavier, J.-F., Hase, F., and Leblanc, T.: H<sub>2</sub>O and δD profiles  
750 remotely-sensed from ground in different spectral infrared regions, *Atmos. Meas.*  
751 *Tech.*, 3, 1599–1613, doi:10.5194/amt-3-1599-2010, 2010.

752 Schoeberl, M. R., Douglass, A. R., Hilsenrath, E., Bhartia, P. K., Barnett, J., Beer, R.,  
753 Waters, J., Gunson, M., Froidevaux, L., Gille, J., Levelt, P. F., and DeCola, P.:  
754 Overview of the EOS Aura Mission, *IEEE T. Geosci. Remote*, 44, 1066-1077, 2006.

755 Shephard, M. W., Herman, R. L., Fisher, B. M., Cady-Pereira, K. E., Clough, S. A.,  
756 Payne, V. H., Whiteman, D. N., Comer, J. P., Vömel, H., Miloshevich, L. M., Forno,  
757 R., Adam, M., Osterman G. B., Eldering, A., Worden, J. R., Brown, L. R., Worden,  
758 H. M., Kulawik, S. S., Rider, D. M., Goldman, A., Beer, R., Bowman, K. W.,  
759 Rodgers, C. D., Luo, M., Rinsland, C. P., Lampel, M., and Gunson, M. R.:  
760 Comparison of Tropospheric Emission Spectrometer (TES) water vapor retrievals  
761 with *in situ* measurements, *J. Geophys. Res.*, 113, D15824,  
762 doi:10.1029/2007JD008822, 2008.

763 Steinwagner, J., Fueglistaler, S., Stiller, G., von Clarmann, T., Kiefer, M., Borsboom, P.  
764 P., van Delden, A., and Rockmann, T.: Tropical dehydration processes constrained by  
765 the seasonality of stratospheric deuterated water, *Nat. Geosci.*, 3, 262-266, 2010.

766 Steinwagner, J., Milz, M., von Clarmann, T., Glatthor, N., Grabowski, U., Hopfner, M.,  
767 Stiller, G. P., and Rockmann, T.: HDO measurements with MIPAS, *Atmos. Chem.*  
768 *Phys.*, 7, 2601-2615, doi:10.5194/acp-7-2601-2007, 2007.

Deleted: in situ

770 Tobin, C. D., Revercomb, H. E., Knuteson, R. O., Lesht, B. M., Strow, L. L., Hannon, S.  
771 E., Feltz, W. F., Moy, L. A., Fetzer, E. J., and Cress, T. S.: Atmospheric Radiation  
772 Measurement site atmospheric state best estimates for Atmospheric Infrared Sounder  
773 temperature and water vapor retrieval validations, *J. Geophys. Res.*, 111, D09S14,  
774 doi:10.1029/2005JD006103, 2006.

775 Urban, J., Lautie, N., Murtagh, D., Eriksson, P., Kasai, Y., Lossow, S., Dupuy, E., de la  
776 Noe, J., Frisk, U., Olberg, M., Le Flochmoen, E., and Ricaud, P.: Global observations  
777 of middle atmospheric water vapour by the Odin satellite: An overview, *Planet. Space*  
778 *Sci.*, 55, 1093-1102, doi:10.1016/j.pss.2006.11.021, 2007.

779 Worden, H. M., Logan, J. A., Worden, J. R., Beer, R., Bowman, K., Clough, S. A.,  
780 Eldering, A., Fisher, B. M., Gunson, M. R., Herman, R. L., Kulawik, S. S., Lampel,  
781 M. C., Luo, M., Megretskaia, I. A., Osterman, G. B., and Shephard, M. W.:  
782 Comparisons of Tropospheric Emission Spectrometer (TES) ozone profiles to  
783 ozonesondes: Methods and initial results, *J. Geophys. Res.*, 112, D03309,  
784 doi:10.1029/2006JD007258, 2007.

785 Worden, J., Bowman, K., Noone, D., Beer, R., Clough, S., Eldering, A., Fisher, B.,  
786 Goldman, A., Gunson, M., Herman, R., Kulawik, S. S., Lampel, M., Luo, M.,  
787 Osterman, G., Rinsland, C., Rodgers, C., Sander, S., Shephard, M., and Worden, H.:  
788 Tropospheric Emission Spectrometer observations of the tropospheric HDO/H<sub>2</sub>O  
789 ratio: Estimation approach and characterization, *J. Geophys. Res.*, 111, D16309,  
790 doi:10.1029/2005JD006606, 2006.

791 Worden, J., Kulawik, S., Frankenberg, C., Payne, V., Bowman, K., Cady-Pereira, K.,  
792 Wecht, K., Lee, J.-E., and Noone, D.: Profiles of CH<sub>4</sub>, HDO, H<sub>2</sub>O, and N<sub>2</sub>O with

793 improved lower tropospheric vertical resolution from Aura TES radiances, *Atmos.*  
794 *Meas. Tech.*, 5, 397–411, doi:10.5194/amt-5-397-2012, 2012.

795 Worden, J. R., Kulawik, S. S., Fu, D., Payne, V. H., Lipton, A. E., Polonsky, I., He, Y.,  
796 Cady-Pereira, K., Moncet, J.-L., Herman, R. L., Irion, F. W., and Bowman, K. W.:  
797 Characterization and evaluation of AIRS-based estimates of the deuterium content of  
798 water vapor, *Atmos. Meas. Tech.*, 12, 2331-2339, [https://doi.org/10.5194/amt-12-](https://doi.org/10.5194/amt-12-2331-2019)  
799 2331-2019, 2019.

800 Worden, J., Kulawik, S., Shephard, M., Clough, S., Worden, H., Bowman, K., and  
801 Goldman, A.: Predicted errors of Tropospheric Emission Spectrometer nadir  
802 retrievals from spectral window selection, *J. Geophys. Res.*, 109, D09308,  
803 doi:10.1029/2004JD004522, 2004.

804 Worden, J., Noone, D., Bowman, K., and TES science team and data contributors:  
805 Importance of rain evaporation and continental convection in the tropical water cycle,  
806 *Nature*, 445, 528-532, doi:10.1038/nature05508, 2007.

807 Worden, J., Noone, D., Galewsky, J., Bailey, A., Bowman, K., Brown, D., Hurley, J.,  
808 Kulawik, S., Lee, J., and Strong, M.: Estimate of bias in Aura TES HDO/H<sub>2</sub>O profiles  
809 from comparison of TES and *in situ* HDO/H<sub>2</sub>O measurements at the Mauna Loa  
810 observatory, *Atmos. Chem. Phys.*, 11, 4491-503, doi: 10.5194/acp-11-4491-2011,  
811 2011.

812 Worden, J., Wecht, K., Frankenberg, C., Alvarado, M., Bowman, K., Kort, E., Kulawik,  
813 S., Lee, M., Payne, V., and Worden, H.: CH<sub>4</sub> and CO distributions over tropical fires  
814 during October 2006 as observed by the Aura TES satellite instrument and modeled  
815 by GEOS-Chem, *Atmos. Chem. Phys.*, 13, 3679–3692, <https://doi.org/10.5194/acp->

Deleted: in situ

817 13-3679-2013, 2013.

818 Wright, J. S., Fu, R., Worden, J. R., Chakraborty, S., Clinton, N. E., Risi, C., Sun, U., and  
819 Yin, L., Rainforest-initiated wet season onset over the southern Amazon, Proc. Nat.  
820 Acad. Sciences, 114, 32, 8481-6, 2017.

821 Zakharov, V. I., Imasu, R., Gribanov, K. G., Hoffmann, G., and Jouzel, J.: Latitudinal  
822 distribution of the deuterium to hydrogen ratio in the atmospheric water vapor  
823 retrieved from IMG/ADEOS data, Geophys. Res. Lett., 31, L12104,  
824 doi:10.1029/2004GL019433, 2004.

825 Zhu, Y., and Gelaro, R.: Observation sensitivity calculations using the adjoint of the  
826 Gridpoint Statistical Interpolation (GSI) analysis system, Mon. Weather Rev., 136,  
827 335-351. doi: 10.1175/MWR3525.1, 2008.

| **Page 14: [1] Deleted** **Robert Herman** **2/18/20 10:02:00 PM**

| **Page 15: [2] Deleted** **Robert Herman** **2/18/20 10:07:00 PM**